Asian Journal of Chemistry; Vol. 26, No. 24 (2014), 8607-8611

ASIAN JOURNAL OF CHEMISTRY

http://dx.doi.org/10.14233/ajchem.2014.18503

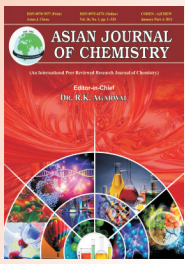

g-C_3N_4/TiO_2 Nanofiber Hybrid Photocatalyst with Effective Photogenerated Charge Separation Rate and Enhanced Activity

Y.F. ZHAO[1,*], J. ZHANG[2], Y.J. WANG[2] and S.Z. HU[3]

[1]School of Environmental and Biological Engineering, Liaoning Shihua University, Fushun 113001, P.R. China
[2]Liaoning Key Laboratory of Petroleum & Chemical Industry, Liaoning Shihua University, Fushun 113001, P.R. China
[3]Institute of Eco-environmental Sciences, Liaoning Shihua University, Fushun 113001, P.R. China

*Corresponding author: E-mail: yanfengzhaolnpu@163.com

Received: 23 July 2014; *Accepted*: 15 September 2014; *Published online*: 1 December 2014; AJC-16415

g-C_3N_4/TiO_2 nanofiber hybrid materials were prepared by a simple hydrothermal method. X-Ray diffraction, UV-visible spectroscopy, scanning electron microscope, electrochemical impedance spectra and X-Ray photoelectron spectroscopy were used to characterize the prepared catalysts. The results indicated that the mass percentage of TiO_2 nanofiber and g-C_3N_4 strongly influenced the optical property and separation efficiency of photogenerated electrons and holes. Ti(0.5)CN(0.5) exhibited the highest photogenerated charge separation rate and the best photocatalytic performance on Rhodamine-B degradation. The reaction rate constant of Ti(0.5)CN(0.5) was 0.004 min^{-1}, which is about 20 and 2 times as high as that of single TiO_2 nanofiber and g-C_3N_4. The possible mechanism was proposed.

Keywords: g-C_3N_4, TiO_2 nanofiber, Charge separation rate, Hybrid materials, Visible light.

INTRODUCTION

Multi-dimensional nanostructures of metals and semiconductors have always attracted material research scientists due to their extensive applications in the field of catalysis, sensing, hydrogen generation, optics and optoelectronics *etc*[1-5]. Titanium dioxide is one special oxide semiconductor that has been widely studied, owing to its multifunctionality. Photocatalysis, dye sensitized solar cells and hydrogen energy production are some of the important fields in which TiO_2 plays a major role[6-10]. Even though TiO_2 is sensitive only to UV-light due to its large band gap (3-3.2 eV), it is still preferred as an ideal candidate to be developed as a visible light active photocatalyst because of its high chemical stability, environmental friendliness and low cost. Development of visible light active TiO_2 has been a major research topic in the past decade. The advancements in the field of visible light active TiO_2, prepared by incorporating various materials such as metals, non-metals and rare earth metals, have been briefly summarized in many review articles[11-13].

Recently, as a metal-free and *n*-type semiconductor, graphite like carbon nitride (g-C_3N_4) with *tris*-triazine units has attracted attentions in the photocatalysis field[14,15]. Benefiting from its special structure, g-C_3N_4 is very stable under light irradiation. Furthermore, the band gap of g-C_3N_4 is about 2.7 eV, indicating that the response wavelength of g-C_3N_4 is up to 460 nm. Although g-C_3N_4 has good visible light response, its UV response is lower than that of TiO_2 and its photogenerated charge separation still need to be improved[16]. To build a heterojunction may be a feasible approach to overcome these disadvantages[17,18]. It is well known that the build-in electric field of heterojunction can drive the photogenerated electrons and holes to transfer to contrary directions, consequently inhibiting their recombination[19]. Moreover, heterojunction composed of two semiconductors can superpose the light response of both semiconductors and therefore, it is possible for the heterojunction to use UV and visible light simultaneously *via* selecting semiconductors with proper band gaps[20].

It is known that the highest occupied molecular orbital (HOMO) of the g-C_3N_4 is located at -1.12 eV and is more negative than the conduction band (CB) of the common wide band gap semiconductor photocatalysts such as TiO_2, ZnO and $BiPO_4$, which is favourable to form heterojunctions with these wide band gap semiconductors and thus to extend their visible light response. Yan *et al.*[21] reported the visible light H_2 evolution using TiO_2/g-C_3N_4 composites prepared through ball milling technique. Zou *et al.*[22] prepared g-C_3N_4 by heating urea in the presence of mesoporous TiO_2 spheres. Miranda *et al.*[23] prepared g-C_3N_4 and TiO_2 hybrid structures by means of a simple impregnation method. However, till now, little attention has been given to prepare g-C_3N_4/TiO_2 nanofiber hybrid photocatalyst. In this work, a novel g-C_3N_4/TiO_2 nanofiber hybrid

photocatalyst was prepared for the first time. The photocatalytic activity was evaluated in the photocatalytic degradation of Rhodamine-B under visible light. The effects of g-C_3N_4/TiO_2 mass ratio on the structural property, optical property and photocatalytic performance of as-prepared catalysts were discussed.

EXPERIMENTAL

In a typical experiment, 4 g melamine was added to 20 mL H_2O under stirring. The obtained suspension was heated to 100 °C to remove the water. The solid product was dry at 90 °C in oven, followed by milling and annealing at 550 °C for 2 h (at a rate of 5 °C min^{-1}). The obtained product was denoted as g-C_3N_4.

0.5 g of tetra-*n*-butyl titanate and 10 M NaOH solution were added to a 50 mL Teflon-lined autoclave. The autoclave was sonicated for 10 min to ensure a complete mixing of the reactants. The autoclave was then heated at 200 °C for 48 h in an electrical oven and gradually cooled down to room temperature. The solid was washed completely with 0.1 M HCl and distilled water, dried in air. The product was denoted as TiO_2 nanofiber. When desired amount of g-C_3N_4 was added into the autoclave following the same procedure as synthesis of TiO_2 nanofiber, the obtained hybrid photocatalyst was denoted as Ti(x)CN(y), where x and y stand for the mass percentage of TiO_2 nanofiber and g-C_3N_4.

X-Ray diffraction patterns of the prepared samples were recorded on a Rigaku D/max-2400 instrument using CuK_α radiation (λ = 1.54 Å). UV-visible spectroscopy measurement was carried out on a JASCO V-550 model UV-visible spectrophotometer, using $BaSO_4$ as the reflectance sample. The morphology of prepared catalyst was observed by using a scanning electron microscope (SEM, JSM 5600LV, JEOL Ltd.). X-Ray photoelectron spectroscopy measurements were conducted on a Thermo Escalab 250 XPS system with Al Kα radiation as the exciting source. The binding energies were calibrated by referencing the C 1s peak (284.6 eV) to reduce the sample charge effect. Electrochemical impedance spectra (EIS) made from these as-made materials were measured *via* an EIS spectrometer (EC-Lab SP-150, Biologic Science Instruments) in a three-electrode cell by applying 10 mV alternative signal versus the reference electrode (SCE) over the frequency range of 1 to 100 MHz. The cyclic voltammograms were measured in 0.1 M KCl solution containing 2.5 mM $K_3[Fe(CN)_6]/K_4[Fe(CN)_6]$ (1:1) as a redox probe with the scanning rate of 20 mV s^{-1} in the same three electrode cell as EIS measurement.

Rhodamine-B was selected as model compound to evaluate the photocatalytic performance of the prepared catalysts in an aqueous solution under visible light irradiation. 0.05 g catalyst were dispersed in 200 mL aqueous solution of Rhodamine-B (10 ppm) in an ultrasound generator for 10 min. The suspension was transferred into a self-designed glass reactor and stirred for 0.5 h in darkness to achieve the adsorption equilibrium. In the photoreaction under visible light irradiation, the suspension was exposed to a 250 W high-pressure sodium lamp with main emission in the range of 400-800 nm and air was bubbled at 130 mL/min through the solution. The UV-light portion of sodium lamp was filtered by 0.5 M $NaNO_2$ solution. All runs were conducted at ambient pressure at 30 °C. At given time intervals, 4 mL suspension was taken and immediately centrifuged to separate the liquid samples from the solid catalyst. The concentrations of Rhodamine-B before and after reaction were measured by means of a UV-visible spectrophotometer at a wavelength of 550 nm.

RESULTS AND DISCUSSION

The XRD patterns of as-prepared g-C_3N_4, TiO_2 nanofiber and Ti(x)CN(y) were displayed in Fig. 1. For g-C_3N_4 contained catalysts, the peak at 27.40° agrees with interlayer stacking of aromatic segments, which is indexed as (002) peak of the stacking of the conjugated aromatic system[24]. For TiO_2 nanofiber contained catalysts, the well-established intensive peak at 25.20° is indexed as (101) plane of anatase TiO_2. Without doubt, the peak intensity of g-C_3N_4 decreased and the peak intensity of TiO_2 increased with increasing the TiO_2 content. The peaks appeared on the XRD patterns of both g-C_3N_4 and TiO_2 can be observed without obvious change. This result indicates that not other crystal phase but the g-C_3N_4/TiO_2 hybrid materials was prepared.

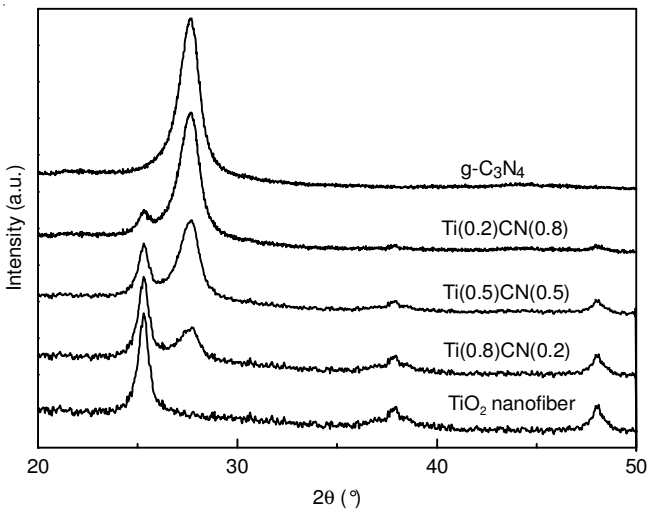

Fig. 1. XRD patterns of as-prepared g-C_3N_4, TiO_2 nanofiber and Ti(x)CN(y)

To study the optical properties of prepared catalysts, UV-visible spectra were measured, as shown in Fig. 2. The absorption intensity starts to increase rapidly at 400 nm for TiO_2, corresponding to the intrinsic band gap absorption of anatase TiO_2. In the case of g-C_3N_4, a typical semiconductor absorption, originating from charge transfer response of g-C_3N_4 from the valence band populated by N 2p orbitals to the conduction band formed by C 2p orbitals. The main absorption edge of g-C_3N_4 occurs at about 470 nm, indicating the band gap energy is about 2.6 eV, which is in good agreement with the value reported in previous literature[25]. For Ti(x)CN(y), the obvious red shift of absorption band was observed with increasing the g-C_3N_4 content. The absorption in visible light region was obviously improved but decreased in ultraviolet light region. The band gap energies for TiO_2, Ti(0.8)CN(0.2), Ti(0.5)CN(0.5) and Ti(0.2)CN(0.8), which calculated according to the method of Oregan and Gratzel were 3.0, 2.88,

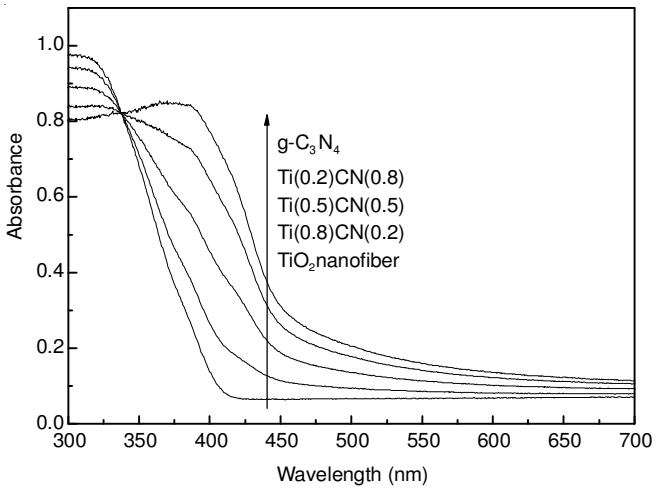

Fig. 2. UV-visible diffuse reflectance spectra of as-prepared g-C_3N_4, TiO_2 nanofiber and Ti(x)CN(y)

2.72 and 2.65 eV[26]. Such decreased band gap energy is favorable to the visible light utilization, thus is favorable to the photocatalytic performance.

The morphology of Ti(0.5)CN(0.5) were examined by using SEM analysis and shown in Fig. 3. The g-C_3N_4 exhibited layered structure, similar to its analogue graphite. This is consistent with previous result[27]. However, the as-prepared TiO_2 showed flower-like nanofiber structure. Besides that, TiO_2 nanofibers seems to grown on g-C_3N_4 substrate. Such intimate interaction between TiO_2 nanofibers and g-C_3N_4 is favorable to the interfacial charge transfer, corresponding to enhanced quantum efficiency.

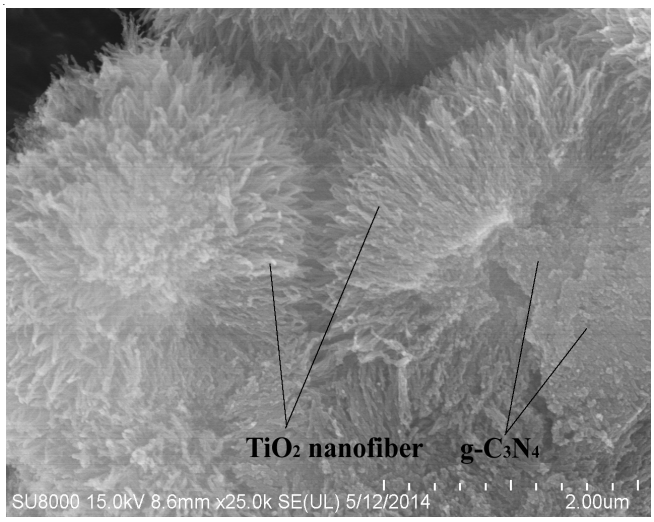

Fig. 3. SEM image of Ti(0.5)CN(0.5)

X-Ray photoelectron spectroscopy is an effective surface test technique to characterize elemental composition and chemical states. Fig. 4 displays the XP spectra of prepared catalysts in the region of Ti 2p (a), O 1s (b), N 1s (c) and C 1s (d). In Ti 2p region (Fig. 4a), both TiO_2 nanofiber and Ti(0.5)CN(0.5) exhibited two peaks which could be assigned to Ti^{4+} $2p_{3/2}$ and Ti^{4+} $2p_{1/2}$ with the binding energy differences, $\Delta E = E$ (Ti $2p_{1/2}$)-E (Ti $2p_{3/2}$), were around 5.7 eV. In Fig. 4b, the peaks around 530.3 and 532.3 eV in the O 1s region are attributed to crystal lattice oxygen (Ti-O) and surface hydroxyl group (O-H) of TiO_2 nanofiber. Ti(0.5)CN(0.5) exhibited the obvious chemical shifts to lower binding energies compared with that of TiO_2 nanofiber in the region of Ti 2p and O 1s, indicating a increase of electron density of Ti and O atoms. This is probably due to the strong interaction between g-C_3N_4 and TiO_2 nanofiber. The electron pair of N in g-C_3N_4 may be partially transferred from to Ti and O, leading to increased electron density. In Fig. 4c and d, the spectra of g-C_3N_4 and Ti(0.5)CN(0.5) in both N 1s and C 1s regions can be fitted with two contributions. For g-C_3N_4, in Fig. 4c, the main N1s peak at a binding energy of 398.6 eV can be assigned to sp^2 hybridized nitrogen (C=N-C), thus confirming the presence of sp^2 bonded graphitic carbon nitride. The peak at higher binding energy 400.6 eV is attributed to tertiary nitrogen [N-$(C)_3$] groups[28]. In Fig. 4d, two components located at 284.6 and 287.8 eV for g-C_3N_4. The sharp peak around 284.6 eV is attributed to the pure graphitic species in the CN matrix. The peak with binding energy of 287.8 eV indicates the presence of sp^2 C atoms bonded to aliphatic amine (-NH_2 or -NH-) in the aromatic rings[29]. In the case of Ti(0.5)CN(0.5), the XPS spectra in N 1s and C 1s regions can also be fitted with two contributions. Besides that, the obvious shift to higher binding energy was observed for Ti(0.5)CN(0.5) in N 1s region but not in C 1s region compared with that of g-C_3N_4. This confirms that the strong interaction between g-C_3N_4 and TiO_2 nanofiber came from the electron transfer from N atoms of g-C_3N_4 to TiO_2 nanofiber.

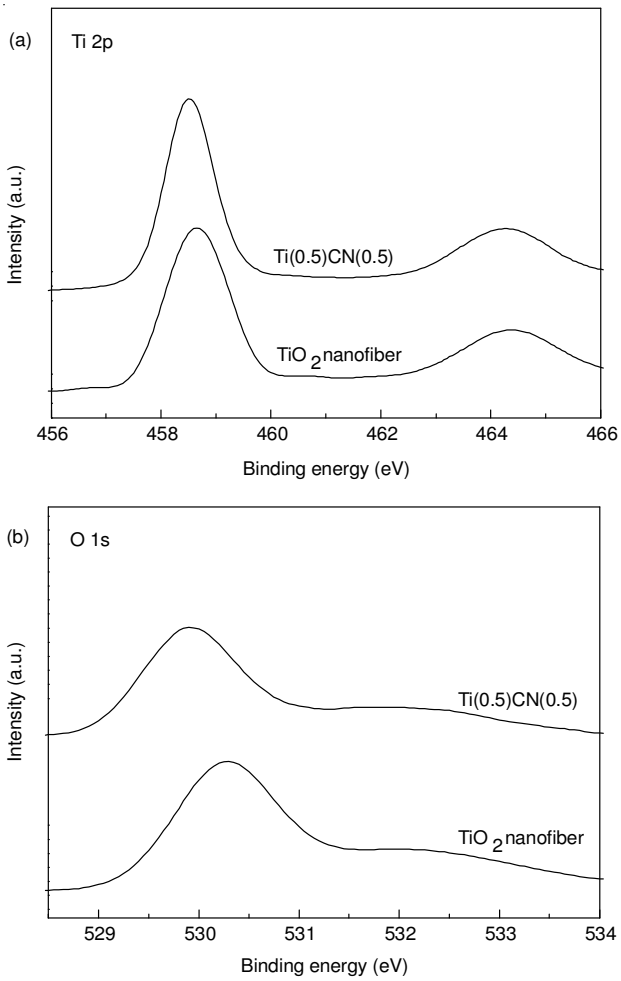

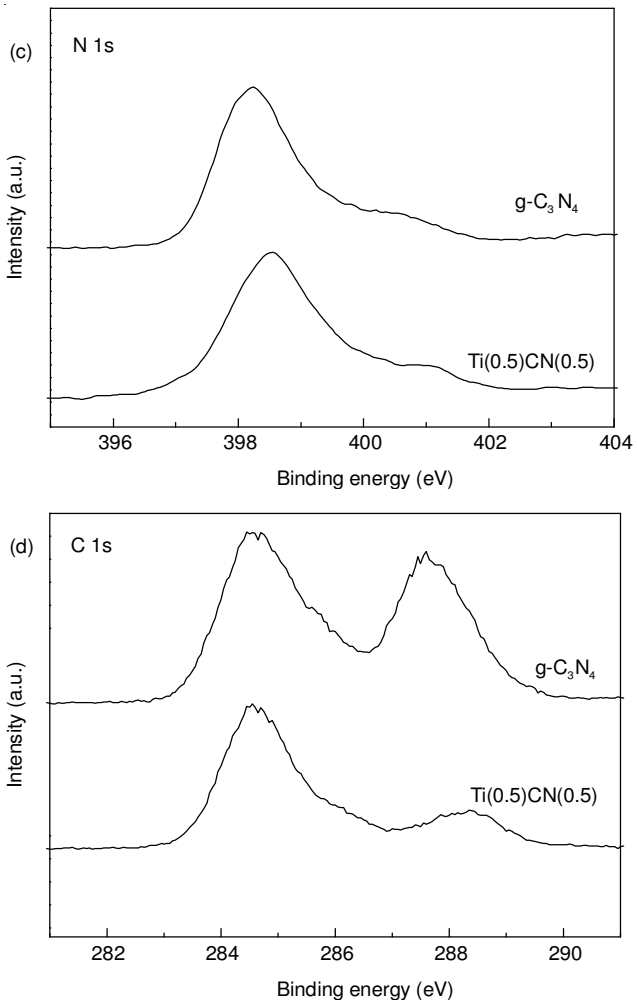

Fig. 4. XP spectra of as-prepared catalysts in the region of Ti 2p (a), O 1s (b), N 1s (c), and C 1s (d)

Electrochemical impedance spectroscopy (EIS) is a useful tool to characterize the charge-carrier migration, thus was used to further confirm the interfacial charge transfer effect of as-prepared Ti(x)CN(y) nanocomposites. Fig. 5 shows the EIS Nyquist plots of the as-prepared g-C_3N_4, TiO_2 nanofiber and Ti(x)CN(y) under visible light irradiation. Obviously, Ti(x)CN(y) shows much decreased arc radius compared with g-C_3N_4 and TiO_2 nanofiber. The reduced arc radius indicates diminished resistance of working electrodes, suggesting a decrease in the solid state interface layer resistance and the charge transfer resistance across the solid-liquid junction on the surface by forming hybrid structures of TiO_2 with g-C_3N_4. Ti(0.5)CN(0.5) shows the smallest arc radius among as-prepared catalysts. Since the radius of the arc on the EIS spectra reflects the migration rate occurring at the surface, it suggests that a more effective separation of photogenerated electron-hole pairs and a faster interfacial charge transfer occurs on Ti(0.5)CN(0.5) surface under this condition.

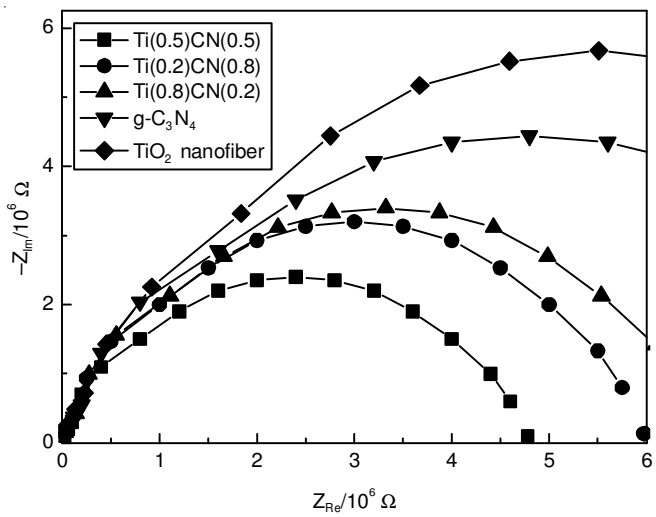

Fig. 5. EIS spectra of as-prepared g-C_3N_4, TiO_2 nanofiber and Ti(x)CN(y)

Fig. 6 shows the photocatalytic performances of as-prepared catalysts under visible light. Control experiment results indicated that the Rhodamine-B degradation occurred only in the existence of both irradiation and photocatalyst. TiO_2 nanofiber exhibited almost no activity, because it can not absorb the visible light directly as shown in Fig. 2. g-C_3N_4 shows a low photocatalytic activity. Only 49 % Rhodamine-B degradation rate is observed. In the case of Ti(x)CN(y), the photocatalytic activities improved obviously compared with that of g-C_3N_4. Ti(0.5) CN(0.5) exhibited the highest activity, about 80 % Rhodamine-B was degraded in 80 min. The photocatalytic activity of mechanical mixing of g-C_3N_4 and TiO_2 nanofiber was also investigated. The result indicated that the activity of mechanical mixing sample was very close to that of single g-C_3N_4 catalyst (~50 %), indicating the improved activity of Ti(x)CN(y) is caused by the strong interaction between g-C_3N_4 and TiO_2 nanofiber. The reaction rate constant k was obtained by assuming that the reaction followed first order kinetics. In a batch reactor, the performance equation is as follows: $-\ln(C/C_0) = kt$ where C_0 and C represent the concentrations of Rhodamine-B dye before and after photocatalytic degradation, respectively. If a linear relationship is established when $-\ln(C/C_0)$ is plotted against t (reaction time), the rate constant k can be obtained from the slope of the line. The calculated results indicated that the rate constant k was 0.0002, 0.0022, 0.0026, 0.004 and 0.0035 min^{-1} for TiO_2 nanofiber, g-C_3N_4, Ti(0.2)CN(0.8), Ti(0.5)CN(0.5) and Ti(0.8)CN(0.2), respectively. Ti(0.5)CN(0.5) exhibited the highest rate constant which is about 2 times and 20 times as high as that of g-C_3N_4

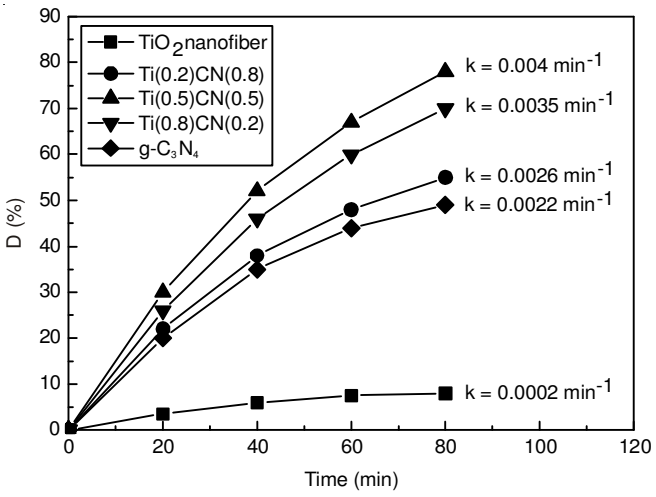

Fig. 6. Photocatalytic performances of as-prepared catalysts under visible light

and TiO_2 nanofiber. Such improved photocatalytic performance is attributed to the improved visible light utilization rate, effective separation of photogenerated electron-hole pairs and a faster interfacial charge transfer.

A possible mechanism for the performance enhancement in Ti(0.5)CN(0.5) composites under visible-light irradiation is depicted in Fig. 7. The conduction band and valence band potentials of TiO_2 were calculated to be -0.3 and +2.9 eV, respectively. In the case of g-C_3N_4, the top of the valence band is +1.57 eV and the bottom of the conduction band is -1.13 eV[30]. Thus, the relative position of potentials was shown in Fig. 7. Under visible-light irradiation, the electrons of g-C_3N_4 are excited from valence band to conduction band. The excited electrons are injected in the conduction band of TiO_2, whose energy is lower than that of the conduction band of g-C_3N_4. Simultaneously, holes are left in the valence band of g-C_3N_4. The photogenerated electrons in the conduction band of TiO_2 will react with O_2 to generate highly active $^{\bullet}O_2^-$ species. It is possible that some photogenerated electrons migrate back to the valence band of g-C_3N_4 to combine with the holes. The energy difference between the valence band of TiO_2 and the valence band of g-C_3N_4 is 1.33 eV, which corresponds to a wavelength of 930 nm. Therefore, electrons in the valence band of TiO_2 can migrate to the valence band of g-C_3N_4 to combine with the residual holes under visible-light irradiation, generating holes in the valence band of TiO_2. The photogenerated holes react with OH^- to form highly active oxygen species $^{\bullet}OH$. The generated $^{\bullet}OH$ and $^{\bullet}O_2^-$ species are responsible for the degradation of Rhodamine-B.

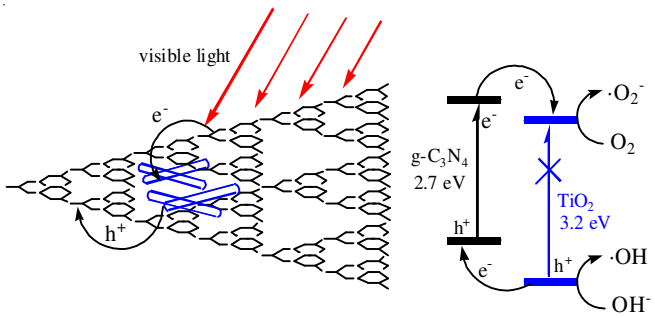

Fig. 7. Mechanism of the photocatalytic degradation over Ti(x)CN(y) under visible light

Conclusion

g-C_3N_4/TiO_2 nanofiber hybrid materials were prepared by a simple hydrothermal method. The mass percentage of TiO_2 nanofiber and g-C_3N_4 strongly influenced the optical property and separation efficiency of photogenerated electrons and holes. SEM result shows that TiO_2 nanofibers grown on g-C_3N_4 substrate. XPS and EIS results indicate that strong interaction between g-C_3N_4 and TiO_2 nanofiber existed which caused more effective separation of photogenerated electron-hole pairs and a faster interfacial charge transfer. Ti(0.5)CN(0.5) exhibited the highest photogenerated charge separation rate and the best photocatalytic performance on Rhodamine-B degradation. The reaction rate constant of Ti(0.5)CN(0.5) was 0.004 min^{-1}, which is ~20 and 2 times as high as that of single TiO_2 nanofiber and g-C_3N_4.

REFERENCES

1. N. Semagina and L. Kiwi-Minsker, *Catal. Rev.*, **51**, 147 (2009).
2. F.S. Kim, G. Ren and S.A. Jenekhe, *Chem. Mater.*, **23**, 682 (2011).
3. A. Vaneski, A.S. Susha, J. Rodríguez-Fernández, M. Berr, F. Jäckel, J. Feldmann and A.L. Rogach, *Adv. Funct. Mater.*, **21**, 1547 (2011).
4. V. Tamilselvan, K. Sridharan, K. Narasimha Rao and R. Philip, *J. Phys. D*, **43**, 385402 (2010).
5. K. Sridharan, V. Tamilselvan, D. Yuvaraj, K. Narasimha Rao and R. Philip, *Opt. Mater.*, **34**, 639 (2012).
6. K. Mori, H. Yamashita and M. Anpo, *RSC Adv.*, **2**, 3165 (2012).
7. I. Paramasivam, H. Jha, N. Liu and P. Schmuki, *Small*, **8**, 3073 (2012).
8. K. Sridharan and T.J. Park, *Appl. Catal. B*, **134-135**, 174 (2013).
9. H. Choi, P.K. Santra and P.V. Kamat, *ACS Nano*, **6**, 5718 (2012).
10. K. Sivaranjani, S. Agarkar, S.B. Ogale and C.S. Gopinath, *J. Phys. Chem. C*, **116**, 2581 (2012).
11. G. Liu, L. Wang, H.G. Yang, H.-M. Cheng and G.Q. (Max) Lu, *J. Mater. Chem.*, **20**, 831 (2010).
12. S. Rehman, R. Ullah, A.M. Butt and N.D. Gohar, *J. Hazard. Mater.*, **170**, 560 (2009).
13. A. Kubacka, M. Fernandez-Garcia and G. Colon, *Chem. Rev.*, **112**, 1555 (2012).
14. X.C. Wang, K. Maeda, A. Thomas, K. Takanabe, G. Xin, J.M. Carlsson, K. Domen and M. Antonietti, *Nat. Mater.*, **8**, 76 (2009).
15. F.Z. Su, S.C. Mathew, G. Lipner, X. Fu, M. Antonietti, S. Blechert and X. Wang, *J. Am. Chem. Soc.*, **132**, 16299 (2010).
16. S.C. Yan, Z.S. Li and Z.G. Zou, *Langmuir*, **26**, 3894 (2010).
17. Y.S. Chen, J.C. Crittenden, S. Hackney, L. Sutter and D.W. Hand, *Environ. Sci. Technol.*, **39**, 1201 (2005).
18. Y.J. Kim, B. Gao, S.Y. Han, M.H. Jung, A.K. Chakraborty, T. Ko, C. Lee and W.I. Lee, *J. Phys. Chem. C*, **113**, 19179 (2009).
19. H.T. Yu, X. Quan, S. Chen and H. Zhao, *J. Phys. Chem. C*, **111**, 12987 (2007).
20. H.T. Yu, S. Chen, X. Quan, H. Zhao and Y. Zhang, *Appl. Catal. B*, **90**, 242 (2009).
21. H.J. Yan and H.X. Yang, *J. Alloys Comp.*, **509**, L26 (2011).
22. X.X. Zou, G.D. Li, Y.N. Wang, J. Zhao, C. Yan, M.Y. Guo, L. Li and J.S. Chen, *Chem. Commun.*, **47**, 1066 (2010).
23. C. Miranda, H. Mansilla, J. Yánez, S. Obregón and G. Colón, *J. Photochem. Photobiol. Chem.*, **253**, 16 (2013).
24. M. Kawaguchi and K. Nozaki, *Chem. Mater.*, **7**, 257 (1995).
25. G.Q. Li, N. Yang, W.L. Wang and W.F. Zhang, *J. Phys. Chem. C*, **113**, 14829 (2009).
26. B. Oregan and M. Gratzel, *Nature*, **353**, 737 (1991).
27. S.Z. Hu, R.R. Jin, G. Lu, D. Liu and J.Z. Gui, *RSC Adv.*, **4**, 24863 (2014).
28. L. Ge and C. Han, *Appl. Catal. B*, **117-118**, 268 (2012).
29. Y.W. Zhang, J.H. Liu, G. Wu and W. Chen, *Nanoscale*, **4**, 5300 (2012).
30. S.C. Yan, S.B. Lv, Z.S. Li and Z.G. Zou, *Dalton Trans.*, **39**, 1488 (2010).